ELSEVIER

Chemical Engineering Journal 142 (2008) 48–55

Chemical Engineering Journal

www.elsevier.com/locate/cej

# Low-temperature $H_2S$ removal from gas streams with SBA-15 supported ZnO nanoparticles

Xiaohui Wang, Tonghua Sun, Ji Yang, Ling Zhao, Jinping Jia *

*School of Environmental Science and Engineering, Shanghai Jiao Tong University, 800 Dongchuan Road, Shanghai 200240, PR China*

Received 21 April 2007; received in revised form 11 November 2007; accepted 12 November 2007

**Abstract**

Mesoporous silica SBA-15 with zinc oxide (ZnO) nanoparticles was prepared via incipient wetness impregnation and ultrasonic method, followed by in situ activation at 523 K. The mesoporous materials obtained were characterized by ICP, XRD, FTIR, nitrogen adsorption, TEM and XPS. The prepared materials showed a superior ability to remove $H_2S$ down to parts per billion (ppb) from gas stream at lower temperature (298 K), and the highest $H_2S$ breakthrough capacity, 436 mg S/g adsorbent, was observed for SBA-15 with 3.04 wt% zinc loading. The enhancement of $H_2S$ removal capacity was attributed to the integration of the high surface area of the mesoporous material and the promising desulphurization properties of ZnO nanoparticles. It was believed that ZnO-modified SBA-15 is a promising adsorbent for $H_2S$ cleaning at ambient conditions, which will extend the application of the mesoporous materials to the environmental protection area.


*Keywords:* Hydrogen sulfide; Removal; Nanoparticle; Mesoporous material

## 1. Introduction

Nowadays strict environmental regulations are driving forces for scientists and engineers to seek efficient and economical ways to remove pollutants either from gaseous or liquid phases [1]. Many industrial processes, such as natural gas processing, petroleum refining, petrochemical plants, kraft mills, coke ovens and coal gasifiers, generate significant quantities of $H_2S$. The removal of $H_2S$ from these gases is necessary to less than few ppm since they are extremely malodorous and toxic, and might poison many industrial catalysts [2,3]. Its oxidation products (sulfur dioxide and sulfur trioxide) are considered to be the sources of acid rain [4]. Furthermore, $H_2S$ in excess of 3 ppmv causes pipeline corrosion and limits plant lifetime [5].

Concerns about $H_2S$ uptake at low temperature are growing because it is by-product of many of industrial processes, such as the Claus process and natural gas sweetening. At low temperature (298–373 K), conventional treatment methods for $H_2S$ treatment for commercial processes include scrubbing, adsorption, and biological treatment [6]. One important topic of current research is the removal of $H_2S$ by adsorption on various porous materials such as activated carbon [7], modified activated carbon [8], γ-$Al_2O_3$, modified clay [9], modified zeolites [10], etc. These porous materials are used extensively as adsorbents, catalyst support and separation media [11]. However, activated carbon suffers drawbacks of low mechanical stability which induces the formation of fines during operation, and high tortuosity with the presence of a large amount of micropores which could hinder the full accessibility of the reactants to the active site [12]. The main drawbacks of $Al_2O_3$ are the chemical interaction between the support and the active phase, leading to the decrease in catalyst performance by chemical reactions and hindering the recovery of the active phase [13]. Microporous materials such as (pillared) clays and zeolites present severe mass transfer limitations when large reactant molecules are involved [14]. Therefore, attempts to improve the diffusion of reactants to the catalytic sites have been focused on increasing the zeolite pore sizes [15], on decreasing zeolite crystal size, or on providing an additional mesopore system within the microporous crystals [16]. A whole field of material research was opened up due to the discovery of mesoporous material, MCM-41 [17] in 1992. The narrow and uniform pore size of mesoporous materials with extremely high surface area holds much promise for the development of novel solid catalysts.

* Corresponding author. Tel.: +86 21 54749910; fax: +86 21 54742817.
*E-mail address:* jpjia2007@163.com (J. Jia).

1385-8947/$ – see front matter © 2007 Elsevier B.V. All rights reserved.
doi:10.1016/j.cej.2007.11.013

In many research applications mesoporous materials already have a comparable and superior performance compared to conventional microporous zeolites or amorphous silica–alumina catalysts. However, reviewing literature, it is fair to say that so far little information on the SBA-15 applications for $H_2S$ gas purifications was available. Therefore, well-ordered, hydrothermally stable mesoporous molecular silica, SBA-15 [18] was selected as $H_2S$ adsorbent media in this study. It is characterized that the intra-wall micropores of SBA-15 form a continuous network that connects adjacent main channels [19]. Such a structure provides an ideal reactor where the mesopore channel acts as a pipe for transport of reactant without significant diffusion resistance and micropores in the walls provide activation sites for reactions [20].

It is known that the performance of $H_2S$ adsorbents depends on their porosity [21] and surface chemistry [22]. Additionally, substitution of elements in the framework, impregnation of active components, and immobilization of active species with pre-determined structure can create well-isolated sites with uniform properties. Therefore, it is an interesting route to improve desulphurization capacity by introducing active phase on mesoporous materials. It has been known that ZnO has high equilibrium constant for $H_2S$ removal at ambient temperature, in the present study, it is for the first time that SBA-15 functionalized by ZnO nanoparticle is prepared through incipient wetness impregnation, ultrasonic treatment and in situ activation route. The mesoporous materials were characterized by TEM, XPS, FTIR, XRD, and $N_2$ adsorption to obtain detailed information in the development of new adsorbents. $H_2S$ desulphurization reaction to form ZnS was chosen as a probe reaction to examine the desulphurization performance of materials synthesized in this study. The factors that have influence on $H_2S$ removal were also discussed. As expected, the material synthesized in this study shows a satisfying desulphurization performance.

## 2. Experiment

### 2.1. Synthesis of mesoporous materials

Triblock poly(ethylene oxide)-*b*-poly(propylene oxide)–*b*-poly(ethylene oxide) copolymer Pluronic P123 (MW = 5800, $EO_{20}PO_{70}EO_{20}$) was purchased from Aldrich. Other chemicals were purchased from Shanghai Zhenxing Chemical Company. All chemicals were used as received.

Twenty grams of P123 was dissolved in 495 g of water and 2 M HCl solution (37 ml) while stirring, and then 45 ml of tetraethyl orthosilicate (TEOS) was added. The obtained suspension was stirred at 313 K for 24 h and then at 373 K for 20 h. The solid product was filtered, washed with distilled water, dried at room temperature, and finally calcined at 823 K for 5 h. The white powder obtained, SBA-15 silica, was used as material for further modification. It is designed as S.

Three hundred millilitres of 2 M sodium carbonate was added in 200 ml of 2 M zinc nitrate with stirring. Then a calculated amount of SBA-15 was added in the suspension, and then treated by ultrasonic machine for 20 min. The mixture was washed by 200 ml of 0.1 M ammonia then 100 ml of absolute ethanol, dried at 353 K for 4 h, and finally calcined at 523 K for 3 h. The sample obtained in this way is designated as S/Z. Sample after desulphurization experiment is designated as S/Z-E.

### 2.2. Characterization of mesoporous materials

A 0.4 g of dry material was added to 20 ml of deionized water, stirred overnight and filtered. The pH value of the solution was measured using an Accumet Basic pH meter (Fisher Scientific, Springfield, NJ). The chemical composing of sample was studied by an Inductive Coupled Plasma (IRIS ADVANTAGE/1000, TJA Corporation, USA). The structural characteristics were determined by Fourier transform infrared spectrophotometer (EQUINOX 55, BRUKER, Germany) (400–4000 $cm^{-1}$). The crystal structures were carried out by X-ray diffractometer (D8Advance, BRUKER, USA; Cu Kα radiation, λ = 1.5406 Å) with a small-angle from 0.5° to 5° and a wide-angle from 10° to 70° before and after desulphurization experiment. The isotherms of nitrogen adsorption/desorption were performed at 77 K using a Gas Absorption Analyzer (TriStar 3000, Micromeritics, USA). The Brunauer–Emmett–Teller (BET) specific surface area was evaluated using adsorption data. The Barrett–Joyner–Halenda (BJH) model [23] was used to determine the pore size distributions from the desorption portion of the isotherm [24]. The surface morphology was checked using a transmission electron microscope (JEM-2100F, JEOL, Japan) with an acceleration voltage of 200 kV. Energy dispersive X-ray (EDX) analysis was performed in an EDAX (Model 6498, Oxford Instruments, England). Binding energies were measured on PHI 5000C ESCA System (PerkinElmer) with Mg Kα radiation ($h\nu$ = 1253.6 eV). Binding energies were calibrated by the carbon (C 1s = 284.6 eV). The data analysis was carried out by using the RBD AugerScan 3.21 software provided by RBD Enterprises.

### 2.3. Desulphurization experiment

The desulfurization experiment was carried out at ambient conditions (298 K, 1 atm). The schematic diagram is presented in Fig. 1. The gaseous mixture at 500 ml/min composed of 0.1% $H_2S$ and balance of air. The gas flow rates were controlled by a mass flow controller system (FMA-700 series controllers coupled with an FMA-78P4 readout/power supply, Omega). Prior to testing, the material was pretreated in flowing He at 303 K to remove the excess moisture and adsorbed impurities from air for 30 min. Adsorbent samples were packed into a U-type glass column (length of 350 mm, diameter of 8 mm). The inlet and outlet gas ($H_2S$) was analyzed by gas chromatograph (Shimadzu, GC2010) equipped with a flame photometry detector (FPD). All outlet gases from the reactor were sampled with an online auto-sampling system and analyzed every minute. The experiment was terminated when outlet $H_2S$ concentration exceeded 50 ppm. In this study, the breakthrough time was defined as the time from the beginning of the desulfurization to the time when the $H_2S$ concentration at the outlet reached 0.1 ppm. The $H_2S$ breakthrough capacity in terms of milligrams of $H_2S$ per gram of material was calculated by integration of the area above

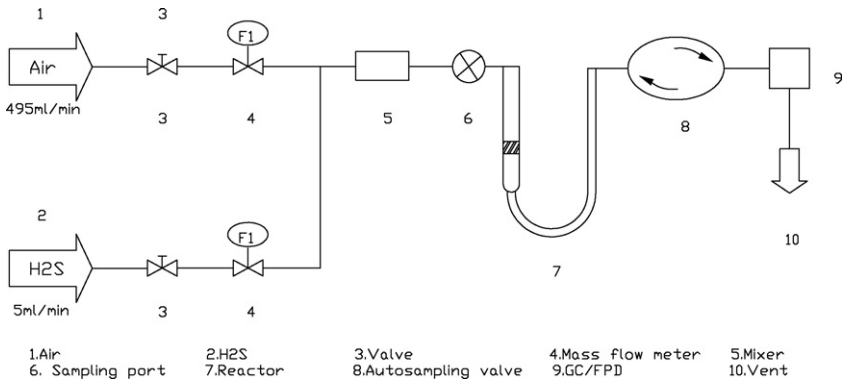


Fig. 1. Schematic representation of desulphurization experimental system.

the breakthrough curve and from the $H_2S$ concentration in the inlet gas, the flow rate, the breakthrough time, and the mass of material.

## 3. Results and discussion

### 3.1. Material characterization

The TEM images of S/Z before and after the desulphurization experiment are presented in Fig. 2. The columnar framework of the SBA-15 material was observed for S/Z, indicating that ordered structure was maintained after modification of ZnO nanoparticle (Fig. 2b). The image of S/Z showed some distortion in the spacing between channels. The particles (black shadow) and the mesopores (white columns) are visible, although they are not very clear. It possibly indicated that ZnO nanoparticle dispersed inside the mesopore. From the image of S/Z-E (Fig. 2d), the particles (the black dot which was tagged by circles) inside the mesopores can be distinguished and dispersed highly on the mesoporous channel of the material. It is possibly the product of desulphurization reaction. Therefore, it can be inferred that ZnO nanoparticle dispersed well in the material and the ultrasonic treatment is an efficient method to scatter guests homogeneously in the hosts.

Fig. 3 shows nitrogen adsorption/desorption isotherms for various samples. Structural properties of materials are depicted in Table 1. For all samples, an approximate type IV isotherm and a $H_1$ type hysteresis loop as defined by IUPAC [25], was observed, which is a characteristic of SBA-15 mesoporous materials with larger pore sizes and narrow size distributions [26,27]. The adsorption branch of each isotherm showed a sharp inflection at $p/p^0 = 0.45$–$0.98$, which means a typical capillary condensation within uniform pores [26]. For both S/Z and S/Z-E, the hysteresis loop with a two-step desorption branch described by Janssen et al. [28] for plugged SBA-15 material is observed. Those are characteristics of inkbottle and cylindrical type mesopores, respectively. The size of the ZnO particles is smaller than the pore diameter. Therefore, it can be inferred that several ZnO particles are probably present in a mesopore, while few ZnO particles are present in other mesopore. The overall amounts of $N_2$ adsorption decrease evidently resulted from the loading of guests (Table 1). It can be explained that ZnO blocked partially the mesopores and mostly micropores. The result is in well harmony with TEM analysis. The remarkable decrease about 45% on surface area and 38% on pore volume of mesopores for S/Z was observed, whereas those of 92% and 93% of micropores, respectively. Therefore, ZnO deposited on both micropores and mesopores, which resulted in the disappearance of micropores and the blockage of mesopore during modification process.

Fig. 4 shows XRD pattern of all samples obtained in this work. In the small-angle range, all samples showed three well-resolved diffraction peaks indexed as (1 0 0), (1 1 0) and (2 0 0) reflections corresponding to *p6mm* hexagonal symmetry, identical to that of SBA-15 [18]. These patterns strongly verified that the characteristic hexagonal features were maintained after $H_2S$ immobilization process. The peaks of S/Z shifted slightly towards bigger angle compared to SBA-15, indicating slight shrinkage in the mesoporous framework possibly due to a higher degree of silicate condensation after ZnO modification. It is in harmony with the data of nitrogen adsorption. In the wide-angle range (Fig. 4b), S/Z gives no obvious diffraction peak corre-

Table 1
Structural property of samples determined by nitrogen adsorption

| Sample | $d_{100}$[a] (nm) | $S_{BET}$ ($m^2$/g) | $S_{mi}$ ($m^2$/g) | $V_{mi}$ ($cm^3$/g) | $V_t$ ($cm^3$/g) | $W_{BJH}$ (nm) | $T_W$[b] (nm) |
|---|---|---|---|---|---|---|---|
| S | 10.0 | 686.7 | 234.6 | 0.099 | 1.64 | 8.2 | 5.5 |
| S/Z | 9.95 | 270.6 | 19.7 | 0.007 | 0.96 | 8.5 | 5.4 |
| S/Z-E | 11.0 | 257.6 | 20.9 | 0.007 | 0.70 | 6.4 | 6.8 |

$V_t$: total pore volume; $V_{mi}$: micropore volume; $S_{BET}$: BET specific area; $S_{mi}$: micropore area; $W_{BJH}$: pore size determined from BJH desorption data; $d$: spacing and primary mesopore volume; $T_W$: wall thickness.

[a] Determined by XRD.

[b] Calculated as follow: $T_W = a_0 - W_{BJH}$.

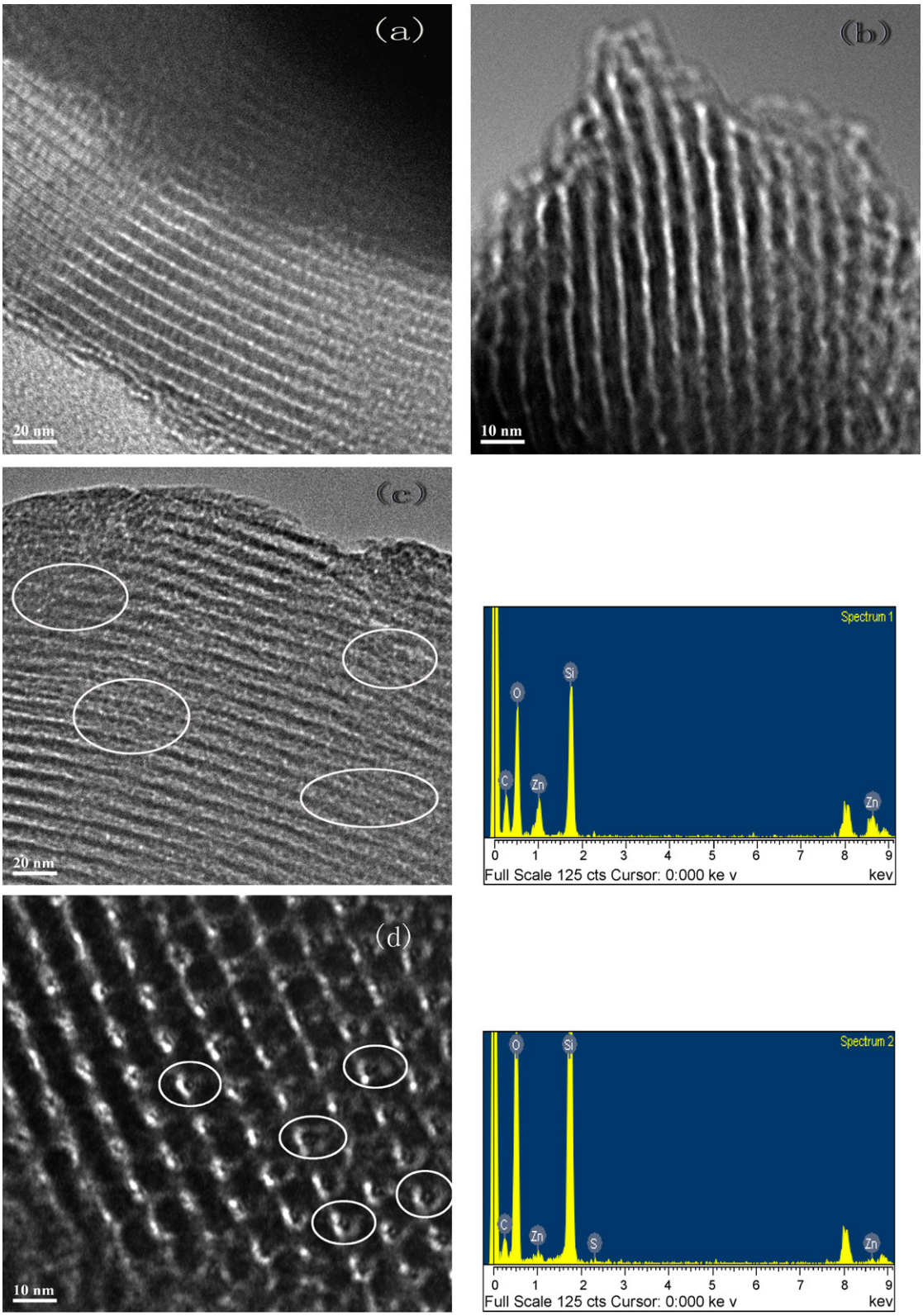


Fig. 2. TEM images of (a) SBA-15, (b) S/Z, S/Z-E taken from the direction (c) vertical and (d) parallel to the channel axis; EDX analysis of the region shown in (c) and (d) corresponding to spectrum 1 and 2, respectively; the Cu peaks result from the use of copper support grid.

sponding to ZnO; such results imply good dispersion of the guests [29] over SBA-15.

The FTIR spectra of the material before and after $H_2S$ desulphurization experiment are provided in Fig. 5. Those bands are assigned to the asymmetric and symmetric stretching vibrations of Si–O–Si framework at 1228, 1080, 801, and 465 $cm^{-1}$ associated with the condensed silica network [30]. The absorbed peaks are associated with non-condensed Si–OH groups in the

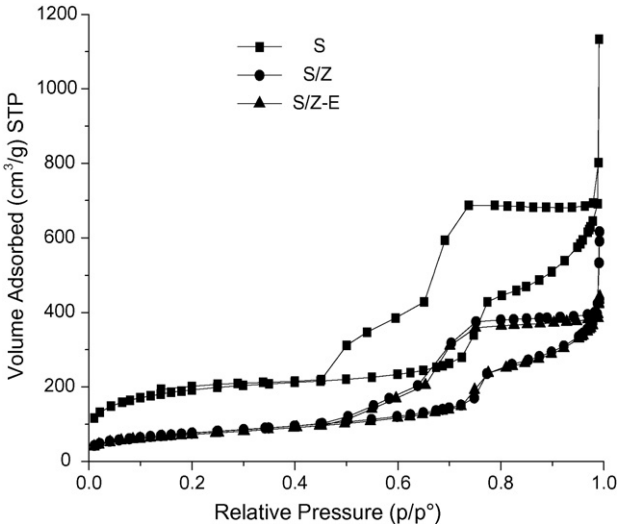


Fig. 3. Nitrogen adsorption–desorption isotherms of S, S/Z, S/Z-E.

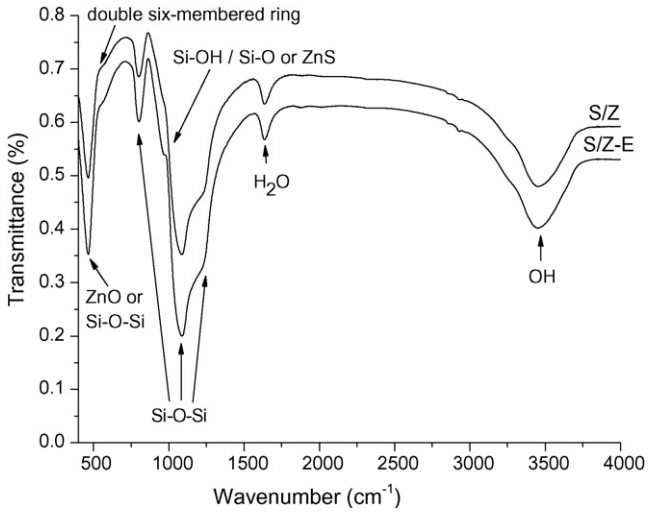


Fig. 5. FTIR spectra of S/Z before and after $H_2S$ desulphurization experiment.

range between 940 and 970 $cm^{-1}$ [31], which are overlapped with that of ZnS. The fairly sharp peak at 466 $cm^{-1}$ region is due to ZnO [32]. The band at 546 $cm^{-1}$ region is associated with double six-membered ring [33], which confirmed the presence of microporous structure. The IR spectrum of carbonate, which is quite characteristic with a very intense broad band centering at 1450 $cm^{-1}$ [34], has not been observed. Therefore, it can be inferred that no carbonate on S/Z was present.

On the basis of the discussion, it can be seen that the material prepared by wetness impregnation and ultrasonic treatment procedures retain the features of mesoporous materials, such as well-order, extremely high surface area, abundant mesoporous and microporous structure, etc.

### 3.2. Desulphurization performance

The desulphurization activity of S/Z was determined using breakthrough capacity measurement described earlier. The breakthrough curves of examples were presented in Fig. 6.

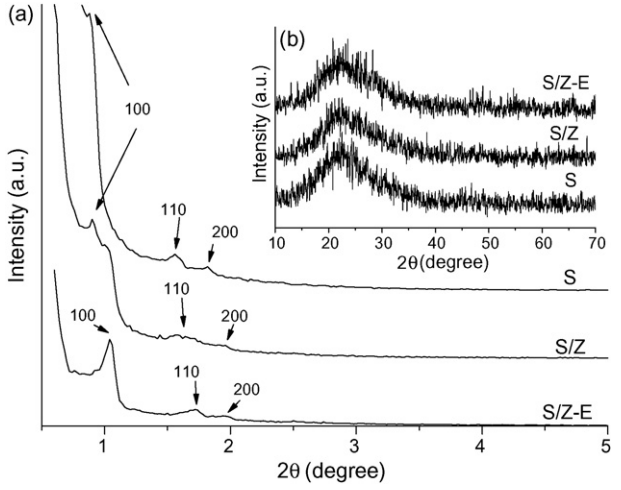


Fig. 4. Small-angle (a) and wide-angle (b) XRD patterns of samples.

The breakthrough capacity of material obtained was reported in Table 2. It is remarkable that outlet $H_2S$ concentration can be effectively controlled below 0.1 ppm before breakthrough point. To understand the role of ZnO on the material desulphurization capacity, zinc content was analyzed. With the increase of ZnO loading, the desulphurization performance of S/Z first increased and then decreased. The 3.04% zinc resulted in significant increase of S/Z-3 performance. The material exhibits a superior affinity to $H_2S$ and the breakthrough capacity is up to 436 mg S/g sorbent. It can be inferred that low ZnO loading results in low desulphurization efficiency. However, excessively high ZnO is also detrimental to the desulphurization reaction. The results possibly suggest that excess of ZnO may block the active centers for desulphurization. It is also possible that besides physical action of 'blocking' active centers, those superabundant ZnO introduces unfavorable chemistry for $H_2S$ desulphurization. Indeed, a perceptible increase of pH is observed with the

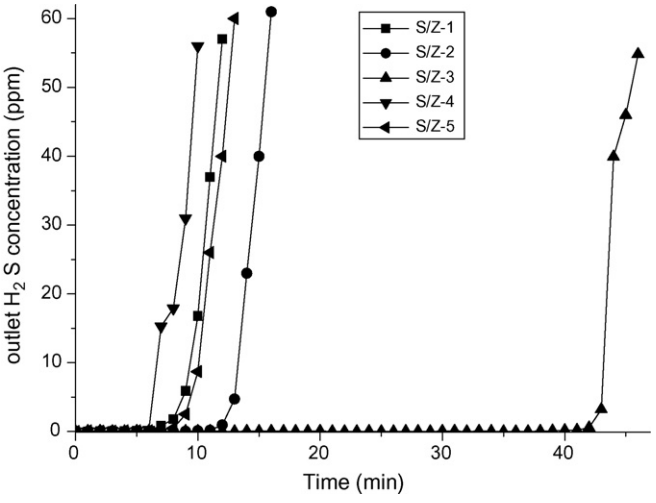


Fig. 6. $H_2S$ breakthrough curves for S/Z with different ZnO loading. Operation condition: 1 atm; 298 K; inlet gas mixture: 0.1 vol% $H_2S$ in air (55% RH); 500 ml/min; mass of adsorbent from S/Z-1 to S/Z-5: 102, 101, 114, 109, 115 mg; the average density of the beds: 105 mg/$cm^3$.

Table 2
$H_2S$ desulphurization capacity and pH values of materials

| Sample | Zn loading (wt %) | Breakthrough time (min) | $H_2S$ breakthrough capacity (mg S/g material) | pH |
|---|---|---|---|---|
| S/Z-1 | 0.50 | 6 | 36.7 | 7.9 |
| S/Z-2 | 1.24 | 10 | 95.0 | 8.2 |
| S/Z-3 | 3.04 | 39 | 436.0 | 8.3 |
| S/Z-4 | 4.45 | 7 | 49.9 | 8.4 |
| S/Z-5 | 9.00 | 6 | 38.9 | 8.7 |

Operation condition: 1 atm; 298 K; inlet gas mixture: 0.1 vol% $H_2S$ in air (55% RH); 500 ml/min; mass of adsorbent from S/Z-1 to S/Z-5: 102, 101, 114, 109, 115 mg; the average density of the beds: 105 mg/cm$^3$.

increase of zinc content. As the reaction progresses, it can be supposed that reaction product was plugging the pores limiting the gas diffusion and, as an outcome, the $H_2S$ capture decreased.

### 3.3. Reaction process analysis

The whole spectra of all the elements and XPS spectra of Zn $2p_{3/2}$ for S/Z and S/Z-E are shown in Fig. 7. A high-resolution XPS curve in the region of 1020–1025 eV was recorded, which shows an intense peak at a binding energy of 1022.5 eV. This peak is characteristic of the $2p_{3/2}$ transition of ZnO [35], indicating the introduction of ZnO into SBA-15. After desulphurization experiment, the BE of Zn $2p_{3/2}$ shifts to a lower region of 1021.8 eV (Fig. 7B) which is assigned to the binding energy of ZnS [36]. To obtain further reaction information, XPS analysis for S $2p_{3/2}$ was also conducted to identify reaction product. As expected, the presence of ZnS was detected at around 162 eV [37]. In addition, the surface atomic percentage ratios derived from XPS data shows that the O/Si atomic ratio of S/Z-E was a greater value than that of the stoichiometric one for $SiO_2$. This discrepancy might be attributed to contribution arising from adsorbed oxygen, whose typical position (at 532.5 eV) is quite close to that of lattice O in $SiO_2$. So, the desulphurization reaction occurred over the material in this study follows the process:

$$ZnO + H_2S \rightarrow ZnS + H_2O.$$

This is supported by TEM and XRD analyses. The image of S/Z-E obtained by TEM showed that material surface became complanate (Fig. 2c) after exposure to $H_2S$/air gas mixture. It can be deduced that reaction product is formed as an overlayer [38] on the surface. XRD results show that the new peak with low intensity appears at 36.1° (Fig. 4b) is assigned to ZnS. The band at 961 cm$^{-1}$ region which is assigned with ZnS for S/Z-E strengthened slightly (Fig. 5), confirming the judgment either (Table 3).

The characterization results of S/Z-E revealed some interesting information. Firstly, XRD pattern of S/Z-E showed that the characteristic hexagonal features were maintained after desulphurization process (Fig. 4a). Furthermore, the peaks of S/Z-E shifted slightly towards bigger angle compared to S/Z, indicating the same trend of slight shrinkage in the mesoporous framework during desulphurization process as that during ZnO modification process. However, it exhibits broader diffraction peaks with lower intensities compared with those of S/Z (Fig. 4b). It is due to a decrease of the crystalline long-range order and is associated with decreasing crystalline domain size and/or accumulated strain [39]. The bands of siliceous framework (Fig. 5) indicated that desulphurization procedure did not induce the collapse of pore structure. From the data of $N_2$ adsorption (Table 1), both

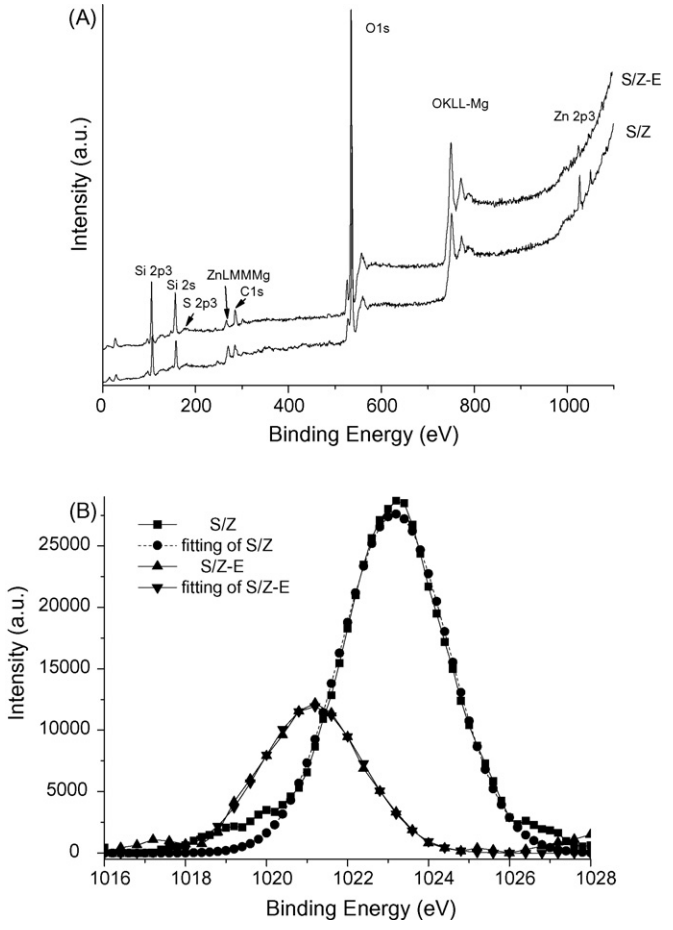


Fig. 7. XPS spectra of the (A) whole spectra and (B) Zn $2p_{3/2}$ narrow spectra for S/Z and S/Z-E.

Table 3
XPS binding energy (eV) of S/Z and S/Z-E

| Sample | O 1s | Si $2p_{3/2}$ | Zn $2p_{3/2}$ | S $2p_{3/2}$ |
|---|---|---|---|---|
| S/Z | 533.3<br>$SiO_2$ | 103.3, 104<br>$SiO_2$ | 1022.5<br>ZnO | –<br>– |
| S/Z-E | 533.2<br>$SiO_2$ | 103.8<br>$SiO_2$ | 1021.8<br>ZnS | 162<br>ZnS |

the surface area and pores volume of mesopores decreased but those of micropores increased slightly for S/Z-E. It seemed that reaction occurred on mesopores. At the same time, the mesopore diameter reduced. Namely, the blockage occurred on mesopores due to the desulphurization product with much bigger crystalline size (the ratio between the molar volume of ZnS and ZnO is 1.6 [40]).

The image taken from the direction parallel to the channel axis (Fig. 2d) of S/Z-E showed clearly the distribution of nanoparticles inside the mesopores. Therefore, the homogeneous distribution of the ZnO nanoparticles inside the pore system contributes a lot to the desulphurization capacity. Besides the fitting mesoporous structure, the outstanding desulphurization capacity is derived from the high surface area which is much higher than commercial ZnO used widely for $H_2S$ capture from gas stream.

From the results of FTIR, XRD and XPS analysis, it can be well assessed that the $H_2S$ removal over SBA-15-supported ZnO at room temperature occurs due to gas–solid reactions in a thin hydrated lattice of metal oxides and ZnS was main product at lower conditions.

## 4. Conclusions

Loading of mesoporous solids with metal oxides is effective by incipient wetness impregnation and ultrasonic treatment, followed by in situ activation procedure. Ultrasonic treatment is an efficient way to scatter guests homogeneously into pores of hosts. The anchor sites of ZnO nanoparticle over SBA-15 synthesized in this study are both mesopores and micropores.

A new $H_2S$ adsorbent consisting of SBA-15 supported ZnO nanoparticles was prepared and studied. This material efficiently removes $H_2S$ from gas streams. The SBA-15-supported material with 3.04% zinc loading shows higher catalytic activity for $H_2S$ removal compared with the commercial desulfurizer.

The as-prepared material has a large number of micropores and mesopores leading to high $H_2S$ adsorption capacity. Another crucial factor is the well-proportioned distribution of active phase inside the mesoporous material. Desulphurization reaction occurred mainly in mesopores and reaction product accumulated in the channels of mesopores and on the surface of adsorbent material.

## References

[1] S.E. Manahan, Environmental Chemistry, 7th ed., CRC Press, Boca Raton, FL, 1997.
[2] M. Capone, J.K. Kroschwitz, M. Howe-Grant (Eds.), Encyclopedia of Chemical Technology, vol. 23, Wiley, New York, 1997, p. 432.
[3] R.Ed. Berkow, The Merck Manual of Diagnosis and Therapy, 16th ed., Merck Research Laboratories, Rahway, NJ, 1992, p. 2691.
[4] H. ter Maat, J.A. Hogendoorn, G.F. Versteeg, The removal of hydrogen sulfide from gas streams using an aqueous metal sulfate absorbent. Part II. The regeneration of copper sulfide to copper oxide—an experimental study, Sep. Purif. Technol. 43 (2005) 199–213.
[5] D. Stirling, The Sulfur Problem: Cleaning up Industrial Feedstocks, The Royal Society of Chemistry, 2000.
[6] D. Gabriel, M.A. Deshusses, Retrofitting existing chemical scrubbers to biotrickling filters for $H_2S$ emission control, Proc. Natl. Acad. Sci. U.S.A. 100 (11) (2003) 6308–6312.
[7] M.A. Daley, C.L. Mangun, J.A.D. Barr, S. Riha, A. Lizzio, G. Donnals, J. Economy, Adsorption of $SO_2$ onto oxidized and heat-treated activated carbon fibers (ACFs), Carbon 35 (1997) 411–417.
[8] A. Bagreev, S. Katikaneni, S. Parab, T.J. Bandosz, Desulfurization of digester gas: prediction of activated carbon bed performance at low concentrations of hydrogen sulfide, Catal. Today 99 (2005) 329–337.
[9] D.N. Thanh, K. Block, T.J. Bandosz, Adsorption of hydrogen sulfide on montmorillonites modified with iron, Chemosphere 59 (2005) 343–353.
[10] M.N. Bae, M.K. Song, Y. Kim, K. Seff, The catalytic activity of vanadium pentoxide film modified electrode on the electrochemical oxidation of hydrogen sulfide in alkaline solutions, Micropor. Mesopor. Mater. 63 (2003) 21–31.
[11] E.A. Khudaish, T.A. Ashraf, The catalytic activity of vanadium pentoxide film modified electrode on the electrochemical oxidation of hydrogen sulfide in alkaline solutions, Electroanal. Chem. 587 (2006) 108–114.
[12] J.-M. Nhut, R. Vieira, L. Pesant, J.-P. Tessonnier, N. Keller, G. Ehret, P.-H. Cuong, M.J. Ledoux, Synthesis and catalytic uses of carbon and silicon carbide nanostructures, Catal. Today 76 (2002) 11–32.
[13] J.A. Schwartz, C. Contescu, A. Contescu, Introduction: heterogeneous catalysis, Chem. Rev. 95 (3) (1995) 475–476.
[14] P.B. Venuto, Organic catalysis over zeolites: a perspective on reaction paths within micropores, Micropor. Mater. 2 (1994) 297–411.
[15] M.E. Davis, C. Saldarriaga, C. Montes, J. Garces, C. Crowder, A molecular sieve with eighteen-membered rings, Nature 331 (1988) 698–699.
[16] I. Schmidt, A. Boisen, E. Gustavsson, K. Stahl, S. Pehrson, S. Dahl, A. Carlsson, C.J.H. Jacobsen, Carbon nanotube templated growth of mesoporous zeolite single crystals, Chem. Mater. 13 (2001) 4416–4418.
[17] C.T. Kresge, M.E. Leonowicz, W.J. Roth, J.C. Vartuli, J.S. Beck, Ordered mesoporous molecular sieves synthesized by a liquid-crystal template mechanism, Nature 359 (1992) 710–712.
[18] D.Y. Zhao, J.L. Feng, Q. Huo, N. Melosh, G.H. Fredrickson, B.F. Chmelka, G.D. Stucky, Triblock copolymer syntheses of mesoporous silica with periodic 50–300 Angstrom pores, Science 279 (1998) 548–552.
[19] M. Kruk, M. Jaroniec, T.-W. Kim, R. Ryoo, Synthesis and characterization of hexagonally ordered carbon nanopipes, Chem. Mater. 15 (2003) 2815–2823.
[20] J.A. Melero, G. Calleja, F. Martínez, R. Molina, Nanocomposite of crystalline $Fe_2O_3$ and CuO particles and mesostructured SBA-15 silica as an active catalyst for wet peroxide oxidation processes, Catal. Commun. 7 (2006) 478–483.
[21] M. Steijns, P. Koopman, B. Nieuwenhuijse, P. Mars, The mechanism of the catalytic oxidation of hydrogen sulfide. III. An electron spin resonance study of the sulfur catalyzed oxidation of hydrogen sulfide, J. Catal. 42 (1976) 96–106.
[22] F. Adib, A. Bagreev, T.J. Bandosz, Effect of pH and surface chemistry on the mechanism of $H_2S$ removal by activated carbons, J. Colloid Interf. Sci. 216 (1999) 360–369.
[23] E.P. Barret, L.G. Joyner, P.H. Halenda, The determination of pore volume and area distributions in porous substances. I. Computations from nitrogen isotherms, J. Am. Chem. Soc. 73 (1951) 373–380.
[24] P.I. Ravikovitch, A.V. Neimark, Characterization of micro- and mesoporosity in SBA-15 materials from adsorption data by the NLDFT method, J. Phys. Chem. B 105 (2001) 6817–6823.
[25] K.S.W. Sing, D.H. Everett, R.A.W. Haul, L. Moscow, R.A. Pierotti, J. Rouquerol, T. Siemieniewska, Reporting physisorption data for gas/solid systems, Pure Appl. Chem. 57 (1985) 603–620.
[26] S.J. Gregg, K.S.W. Sing, Adsorption, Surface Area, and Porosity, Academic Press, London, 1982.
[27] D.Y. Zhao, Q.S. Huo, J.L. Feng, B.F. Chmelka, G.D. Stucky, Nonionic triblock and star diblock copolymer and oligomeric surfactant syntheses of highly ordered, hydrothermally stable, mesoporous silica structures, J. Am. Chem. Soc. 120 (1998) 6024–6036.
[28] A.H. Janssen, C.M. Yang, Y. Wang, F. Schueth, A.J. Koster, K.P.D. Jong, Localization of small metal (oxide) particles in SBA-15 using bright-field electron tomography, J. Phys. Chem. B 107 (2003) 10552–10556.

[29] A. Auroux, A. Gervasini, C. Guimon, Acidic character of metal-loaded amorphous and crystalline silica-aluminas determined by XPS and adsorption calorimetry, J. Phys. Chem. B 103 (1999) 7195–7205.
[30] A. Lapkin, B. Bozkaya, T. Mays, L. Borello, K. Edler, B. Crittenden, Preparation and characterization of chemisorbents based on heteropoly-acids supported on synthetic mesoporous carbons and silica, Catal. Today 81 (2003) 611–621.
[31] H. Günzler, H.-U. Gremlich, IR Spectroscopy, Wiley–VCH, Weinheim, Germany, 2002.
[32] K.D.O. Jackson, A Guide to Identifying Common Inorganic Fillers and Activators Using Vibrational Spectroscopy, 3rd ed., vol. 2, The Internet Journal of Vibrational Spectroscopy, 1998.
[33] X. Zhang, Synthesis of 13X molecular sieve from potassium feldspar (in Chinese), China Univ. Geosci. 22 (2003) 167–172.
[34] Q. Sun, S.F. Weng, X. Zhang, FTIR microanalysis limits of hydrocarbon fluid inclusions: matrix minerals absorption, Earth Sci.-J. China Univ. Geosci. 23 (1998) 248–252.
[35] S.W. Gaarenstroom, N. Winograd, J. Chem. Phys. 67 (1977) 3500.
[36] L.S. Dake, D.R. Baer, J.M. Zachara, Surf. Interf. Anal. 14 (1989) 71.
[37] B.R. Strohmeier, D.M. Hercules, J. Catal. 86 (1984) 266.
[38] J.M. Davidson, C.H. Lawrie, K. Sohail, Kinetics of the absorption of hydrogen sulfide by high purity and doped high surface area zinc oxide, Ind. Eng. Chem. Res. 34 (1995) 2981–2989.
[39] M.A. Ahmed, E. Garcia, L. Alonso, J.M. Palacios, A MS, SEM-EDX and XRD study of Ti or Cu-doped zinc ferrites as regenerable sorbents for hot coal gas desulfurization, Appl. Surf. Sci. 156 (2000) 115–124.
[40] S.C. Christoforou, E.A. Efthimiadis, I.A. Vasalos, Sulfidation of mixed metal oxides in a fluidized-bed reactor, Ind. Eng. Chem. Res. 34 (1995) 83–93.